Appropriate Formulation of the Characteristic Equation for Open Nonreciprocal Layered Waveguides With Different Upper and Lower Half-Spaces

Raúl Rodríguez-Berral, Francisco Mesa, *Member, IEEE*, and Francisco Medina, *Senior Member, IEEE*

***Abstract*—This paper will study the most convenient way of formulating the characteristic equation for shielded, parallel-plate, grounded, and open reciprocal/nonreciprocal planar layered waveguides, including the possibility of different upper and lower half-spaces. A detailed study of the suitable mapping for each kind of waveguide will lead to the formulation of *analytic* characteristic equations for shielded/parallel-plate/grounded reciprocal/nonreciprocal waveguides and also for open reciprocal ones. Although no mapping has been found to remove all the branch points of the characteristic equation for open nonreciprocal waveguides with different half-spaces, a robust approach will be proposed to overcome the main drawbacks caused by the multivalued nature of this problem. The combination of the suitable formulation of the characteristic equation with a systematic integral-nature root-searching strategy bears a reliable and efficient method. Some novel numerical results will be presented for open anisotropic reciprocal waveguides and for open magnetized ferrite slabs to illustrate the performance of the present proposal.**

***Index Terms*—Leaky waves, nonreciprocal wave propagation, planar waveguides, root loci.**

I. Introduction

PLANAR layered waveguides are of great interest in microwave engineering and optics because of their use as the background structure for integrated circuitry. Hence, from early on, much effort has been devoted to study the propagation characteristics of the modal spectrum of these waveguides [1]–[27]. Additionally, that study is key to determine the characteristics of the Green's function involved in the solution of scattering and propagation problems for antennas and high-frequency printed circuits by means of the integral-equation method. Specifically, the propagation constants of the waveguide determine the singularities of the spectral-domain Green's function [9], and are also required in obtaining accurate closed-form expressions for the space-domain Green's functions [28], [29]. Thus, numerous and diverse approaches have been proposed to deal with different kinds of planar waveguides: shielded, laterally open, and grounded reciprocal/nonreciprocal waveguides [2]–[12], [15], [16], [19]–[24], [27]. Planar waveguides opened to both (and eventually different) upper and lower half-spaces, henceforth, *open* planar waveguides, have also been analyzed, e.g., in [13], [17], [18], [20], [23], [25], [26]. Nevertheless, to the authors' knowledge, previous studies have not considered the case of open waveguides whose layered substrate includes nonreciprocal materials (the case of open reciprocal anisotropic waveguides treated in [26] was restricted to anisotropic dielectric slabs in free space). The rich phenomenology provided by gyrotropic (e.g., magnetized ferrites) substrates in an open environment could be of potential practical interest to design, e.g., new types of radiators [30]–[32].

The great variety of approaches reported in the literature to study each specific type of planar waveguide can make it difficult to draw a general view of the problem under consideration, and to achieve a clear understanding of the similarities and differences existing between the application of a given approach to each kind of waveguide. Hence, this study will attempt to collect all of the possible different cases of planar layered waveguides, including the open nonreciprocal case, with the purpose of giving a general perspective of them within a congruent and efficient approach.

The problem of finding the modal propagation constants of open planar layered waveguides will be reduced to a root-searching procedure in a similar way as was done in [19] for grounded structures. That paper posed a corresponding eigenvalue problem whose characteristic equation provided a formulation of the waveguide dispersion relation as the complex zeros of a complex function free of poles and branch points. The treatment of this eigenvalue problem will be extended here to deal with the case of open waveguides with different upper and lower half-spaces. Moreover, this paper will also study how the peculiarities of each kind of waveguide demands to pose its corresponding characteristic equation in a different and more appropriate mathematical form. Specifically, the further removal of the possible branch-point singularities of the characteristic function will be key to build a robust and reliable algorithm based on root-searching procedures. As is well known, these latter procedures do not work properly in those regions of the complex plane where the function is not

Manuscript received July 15, 2004. This work was supported by the Spanish Ministry of Education and Science and by FEDER funds under Project TEC2004-03214.

R. Rodríguez-Berral and F. Mesa are with the Grupo de Microondas, Departamento de Física Aplicada 1, ETS de Ingeniería Informática, Universidad de Sevilla, 41012-Seville, Spain (e-mail: mesa@us.es).

F. Medina is with the Grupo de Microondas, Departamento de Electrónica y Electromagnetismo, Universidad de Sevilla, 41012-Seville, Spain (e-mail: medina@us.es).

Digital Object Identifier 10.1109/TMTT.2005.847051

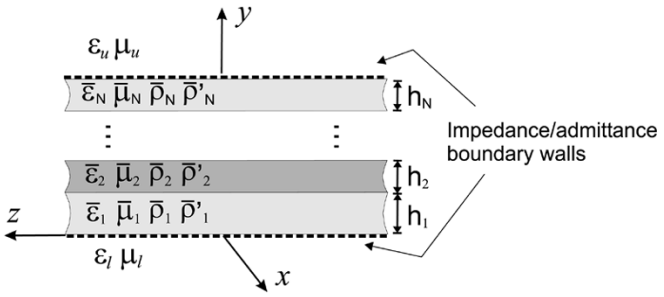

Fig. 1. Cross section of the planar N-layers waveguide under study. The structure is infinite in both the x- and z-directions, and can be bounded by electric/magnetic walls or different lower and upper half-spaces.

analytic (it should be reminded that only analytic functions are complex differentiable at every point of the region). In this sense, a general discussion on the mappings that could succeed in removing the possible branch points of the characteristic function will be carried out for each kind of waveguides. As a result, the characteristic functions proposed in this study will be analytic for any kind of structure, except for the case of open nonreciprocal waveguides. Nevertheless a new robust approach will also be proposed for this latter case in spite of not having found a mapping to unfold the associated Riemann surface. The numerical efficiency of this proposal is also conveniently enhanced by the use of a integral-nature root-searching procedure [33], [34] following the systematic strategy reported in [27].

This paper is organized as follows. Section II will briefly outline the mathematical formulation of the problem. Section III will expose the scheme used to deal with reciprocal waveguides. This section will distinguish between the treatment for parallel-plate and/or grounded waveguides and that for open waveguides. Finally, the study of nonreciprocal structures will be presented in Section IV, also differentiating the grounded and open cases.

II. Formulation of the Problem

The planar waveguide under consideration (see Fig. 1) is composed of N layers having the following general linear constitutive relations:

$$\begin{cases} \mathbf{D}_i = \bar{\varepsilon}_i \cdot \mathbf{E}_i + \bar{\rho}_i \cdot \mathbf{H}_i, \\ \mathbf{B}_i = \bar{\rho'}_i \cdot \mathbf{E}_i + \bar{\mu}_i \cdot \mathbf{H}_i, \end{cases} \qquad i = 1, \ldots, N \tag{1}$$

where $\bar{\varepsilon}$, $\bar{\mu}$, $\bar{\rho}$, and $\bar{\rho'}$ are the (3×3) complex tensors accounting, respectively, for the electric permittivity, magnetic permeability, and optical activity. The upper and bottom boundaries of the waveguide can be electric and/or magnetic walls, and free-space and/or dielectric half-spaces. (The theory proposed here will also be able to deal with any type of boundary condition susceptible to be implemented in the spectral domain by means of impedance/admittance dyadics. This would also include, for example, the cases of lossy conductors under the approximation of the surface impedance, periodic boundary conditions, etc.)

Assuming a common dependence of the fields of the type $F(x,y,z,t) = F(y)\exp[-j(k_x x + k_z z - \omega t)]$, and following [7], [9], [19], and [35]–[37], the transverse-to-y fields at the upper and lower interfaces ($\mathbf{X}^u$ and $\mathbf{X}^l$) can be related by $\mathbf{X}^u = [\mathbf{A}] \cdot \mathbf{X}^l$, where $\mathbf{X} = (E_x, E_z, H_x, H_z)$, and $[\mathbf{A}]$ is a (4×4) matrix that depends only on k_x, k_z, ω, and the characteristics of the layered substrate. The introduction of the corresponding upper and lower impedance/admittance boundary conditions allows us to write the following characteristic equation [19]:

$$\det[\mathbf{L}(k_x, k_z, \omega)] = 0 \tag{2}$$

where the (2×2) matrix $[\mathbf{L}]$ is given by

$$[\mathbf{L}] = [\mathbf{A}_{12}] - [\mathbf{Z}_u] \cdot [\mathbf{A}_{22}] + \big([\mathbf{A}_{11}] - [\mathbf{Z}_u] \cdot [\mathbf{A}_{21}]\big) \cdot [\mathbf{Z}_l] \tag{3}$$

with $[\mathbf{A}_{ij}]$ being the (2×2) submatrices of matrix $[\mathbf{A}]$ and $[\mathbf{Z}_u], [\mathbf{Z}_l]$ the upper and lower impedance matrices. (Other equivalent formulations are possible, also involving the admittance matrices instead of the impedance ones.) In the following, and without loss of generality, the x- and z-axes orientation will be chosen such that propagation always takes place along the x-direction assuming $k_z = 0$ (for periodic or laterally shielded structures, k_z should be taken so as to satisfy the corresponding lateral boundary conditions). For isotropic and/or anisotropic/gyrotropic materials with their main axis along the y-direction, the above assumption is irrelevant since the x- and z-directions are completely equivalent. For more general cases, a change in x- and z-axes orientation would only imply a rotation of the characteristic tensors around the y-axis.

III. Reciprocal Waveguides

Before discussing the formulation of the dispersion equation for reciprocal planar waveguides, it is convenient to note that the reciprocity of these structures causes the elements of matrix $[\mathbf{A}]$ to be invariant under inversion of the propagation direction; namely, they are even functions of k_x. In addition, the uniqueness theorem assures that the fields at any point within the multilayer are uniquely determined by the transverse fields at the lower interface. As a consequence, the elements in matrix $[\mathbf{A}]$ are single-valued functions of k_x^2 and, therefore, the branch points of the characteristic function (if any) will arise from the impedance matrices. Finally, it should be recalled that the elements of matrix $[\mathbf{A}]$ do not have poles for any specific form of the characteristic tensors [19], whereas the elements of the impedance matrices are even functions of k_x for half-space boundary conditions [38].

A. Parallel-Plate and Grounded Reciprocal Waveguides

Since parallel-plate waveguides have null upper and lower impedance matrices, the characteristic function for this case can be written as

$$F_1\left(k_x^2, \omega\right) = \det[\mathbf{L}\left(k_x^2, \omega\right)] \tag{4}$$

which is fully analytic in the complex k_x^2-plane. Thus, there is no need for a mapping in order to use other computational variables (i.e., the independent variable in which the characteristic equation is finally posed) than k_x^2—the square of the longitudinal wavenumber k_x. The root-searching strategy presented in [27] can then be straightforwardly applied to the characteristic function in (4). (The choice for the computational variable reported in [27] would not make sense for anisotropic reciprocal

waveguides because of the presence of ordinary and extraordinary rays.)

For grounded structures, the determinant of matrix $[\mathbf{L}]$ does present a branch point in the complex k_x^2 plane at $k_x^2 = k_u^2$ [38], where $k_u^2 = \omega^2\varepsilon_u\mu_u$ with ε_u and μ_u being the permittivity and permeability of the upper half-space, respectively (grounded waveguides will be always considered to have null impedance at the lower interface). The two-sheeted nature of the Riemann surface defined in the complex k_x^2 plane comes from the two possible choices in the sign of the vertical wavenumber in the upper half-space, $k_{yu} = \pm\sqrt{k_u^2 - k_x^2}$ for each value of k_x^2. Taking into account the even nature of the elements in matrices $[\mathbf{A}]$ and $[\mathbf{Z}_u]$, it can be asserted that the mapping

$$k_{yu} = \sqrt{k_u^2 - k_x^2} \tag{5}$$

will remove the branch points for reciprocal grounded waveguides. Thus, the following analytic characteristic function is proposed:

$$F_2(k_{yu}, \omega) = k_{yu}\det\big[\mathbf{L}(k_{yu}, \omega)\big] \tag{6}$$

where the multiplicative factor k_{yu} has been introduced to remove the pole at $k_{yu} = 0$ arising from the upper half-space impedance matrix.

B. Open Reciprocal Waveguides

For open reciprocal waveguides, $\det[\mathbf{L}]$ has two branch points in the complex k_x^2-plane located at $k_x^2 = k_u^2$ and $k_x^2 = k_l^2$ [13], [17], [18], [20], where $k_l^2 = \omega^2\varepsilon_l\mu_l$ with ε_l and μ_l being the lower half-space permittivity and permeability. The reason for the new branch point comes from the ambiguity in the sign of the vertical wavenumber in the lower half-space $k_{yl} = \pm\sqrt{k_l^2 - k_x^2}$. Hence, the complex k_x^2-plane is now a Riemann surface that comprises four sheets, one for each combination of the signs of k_{yu} and k_{yl}. In order to find a mapping that unfolds this Riemann surface, the new variable should be chosen as a combination of k_{yu} and k_{yl} so that it contains all the information concerning the signs of these two variables. Looking for simple combinations, the product of k_{yu} and k_{yl} must be discarded because it takes the same value for different combination of signs, e.g., $(-k_{yu})(-k_{yl}) = k_{yu}k_{yl}$. The same can be adduced for k_{yu}/k_{yl}, which, in addition, has a singular point at $k_{yl} = 0$. Therefore, the following linear combination of these two variables will be next considered and examined:

$$f(\xi) = c_1 k_{yu} + c_2 k_{yl} \tag{7}$$

where $f(\cdot)$ is a given analytic function and c_1, c_2 are two complex constants. For this mapping to unfold the Riemann surface, there must be an unique value of both k_{yu} and k_{yl} corresponding to each value of ξ. In other words, both k_{yu} and k_{yl} must be single-valued functions of ξ. Taking into account that $k_{yu}^2 = k_{yl}^2 - R^2$, where $R^2 = k_l^2 - k_u^2$, mapping (7) can be written as

$$\left[c_1^2 - c_2^2\right]k_{yl}^2 + \left[2f(\xi)c_2\right]k_{yl} - \left[f^2(\xi) + c_1^2R^2\right] = 0 \tag{8}$$

which is a second-order complex polynomial in k_{yl}. In consequence, there are two values of k_{yl} corresponding to each value of ξ unless $c_1 = \pm c_2$. Thus, considering the latter relation between c_1 and c_2, mapping (7) must have the form

$$f(\xi) = k_{yu} \pm k_{yl} \tag{9}$$

thus leading to the following single-valued expression of k_{yl} as a function of ξ:

$$k_{yl} = \pm\frac{1}{2}\left[f(\xi) + \frac{R^2}{f(\xi)}\right]. \tag{10}$$

It should be noted that the $\pm$ sign in (10) does not indicate any ambiguity in the sign of k_{yl}, but is simply the sign choice in (9). Looking at (10), it can be concluded that an important feature to be satisfied by function $f(\xi)$ is that this function must not have zeros for any finite value of ξ (otherwise, k_{yl} would diverge because of the appearance of a singular point in the mapping). The previous analysis involving variable k_{yl} can be also equivalently carried out using variable k_{yu}, leading to the same requirements for c_1, c_2, and $f(\xi)$. The expression of k_{yu} as a function of ξ is found to be

$$k_{yu} = \frac{1}{2}\left[f(\xi) - \frac{R^2}{f(\xi)}\right]. \tag{11}$$

It can then be concluded that any mapping having the form given in (9), with $f(\xi)$ being an analytical function without zeros, is regular and removes the branch points of the characteristic function for open reciprocal waveguides. For example, the family of mappings proposed in [20] is a particular case of the general mapping in (9). Our specific choice will be

$$Re^{j\xi} = k_{yu} + k_{yl} \tag{12}$$

which is actually very similar to that proposed in [18]. Nevertheless, it should be pointed out that our proposal has followed a different rationale that can complement the previous discussions on this subject. Using (12), the expressions relating k_{yu} and k_{yl} to ξ are

$$k_{yl} = R\cos(\xi) \tag{13}$$

$$k_{yu} = jR\sin(\xi) \tag{14}$$

$$\xi = -j\ln\left(\frac{k_{yu} + k_{yl}}{R}\right) \tag{15}$$

which would lead to the following analytic expression of the characteristic function for these structures:

$$F_3(\xi, \omega) = \cos(\xi)\sin(\xi)\det\big[\mathbf{L}(\xi, \omega)\big] \tag{16}$$

where the determinant of matrix $[\mathbf{L}]$ has been multiplied by $\cos(\xi)$ and $\sin(\xi)$ in order to remove the poles at $k_{yu} = 0$ and $k_{yl} = 0$ arising from the upper and lower impedance matrices. The basic reason for our proposal (12) is that it leads to a straightforward mapping of the different sheets of the original Riemann surface onto the complex ξ plane (see Fig. 2). Since the complex logarithm is a multivalued function with an infinite number of branches, there will be an infinite number of values of ξ corresponding to each pair of values of k_{yu} and k_{yl} [18],

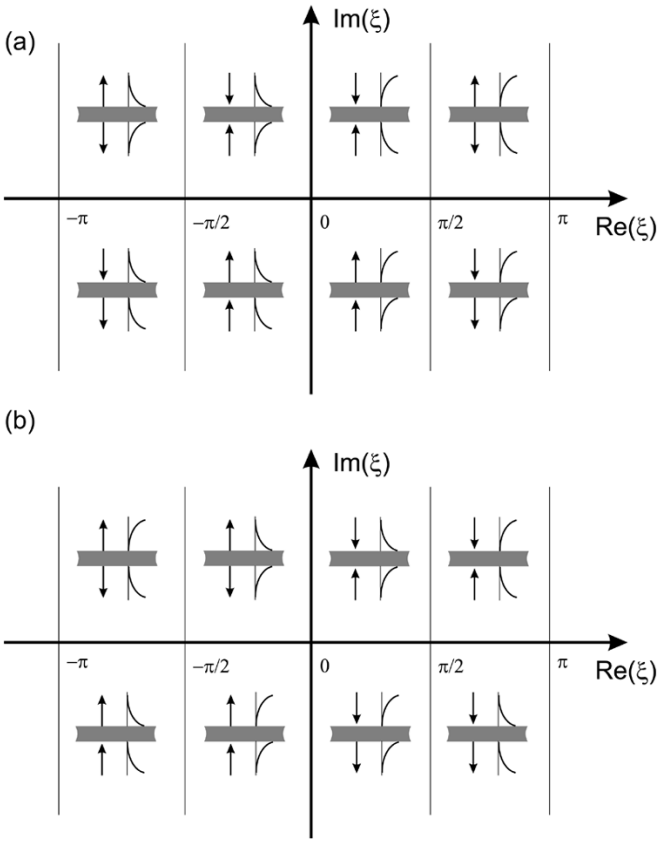

Fig. 2. Schematic representation of the mapping in (12) for: (a) $k_l > k_u$ and (b) $k_u > k_l$. In each zone of the region of interest of the complex ξ-plane, the power flow along the vertical direction is indicated by arrows and the exponential behavior of the fields by increasing/decreasing curves.

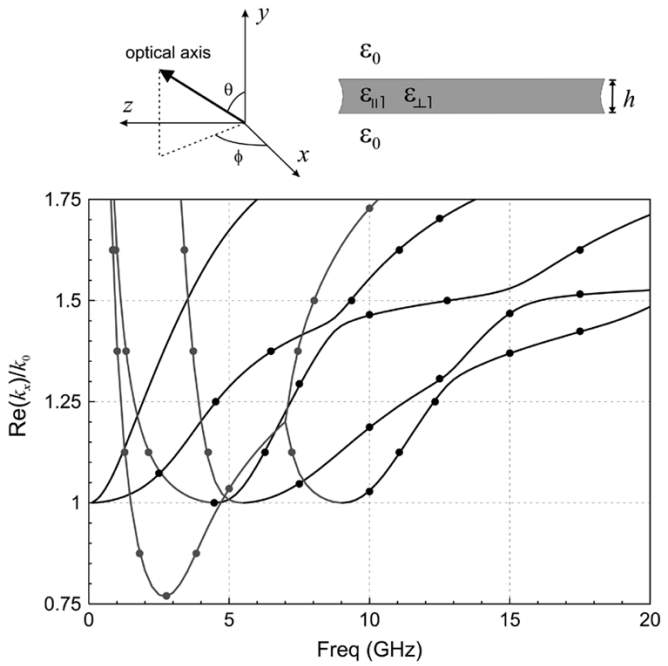

Fig. 3. Normalized phase constants of the first modes of an open anisotropic planar slab, previously analyzed in [26, Fig. 2] with $h = 2$ cm, $\varepsilon_{\|1} = 2.25\varepsilon_0, \varepsilon_{\perp 1} = 4\varepsilon_0$, and the optical axis oriented with $\theta = 45°, \phi = 60°$. Solid lines: our results. Points: data in [26]. Black color lines and points stand for proper modes, grey color for improper modes.

[20]. However, this fact does not pose any troubles provided that the principal value of the logarithm is always taken, thus, restricting the ξ domain to $-\pi < \Re(\xi) \leq \pi$. The eight zones of Fig. 2 have been labeled in a manner similar to [18]: the arrows represent the power flow along the vertical direction, whereas the curves represent the exponential behavior of the fields. Note that the mapping depends on whether $k_l > k_u$ or $k_u > k_l$ because R will be respectively real or imaginary (in both cases, the nonzero part of R is chosen to be positive). Bound modes (BMs) in lossless waveguides must have k_{yu} and k_{yl} both imaginary with $\Im(k_{yu}) < 0$ and $\Im(k_{yl}) > 0$ and, therefore, they will be located on the $[\Re(\xi) = -\pi/2, \Im(\xi) > 0]$ segment of the complex ξ-plane for $k_l > k_u$ and on $[\Re(\xi) = 0, \Im(\xi) > 0]$ for $k_u > k_l$. As losses increase, BMs will move from their original location to the right entering the $[-\pi/2 < \Re(\xi) < 0, \Im(\xi) > 0]$ and $[0 < \Re(\xi) < \pi/2, \Im(\xi) > 0]$ zones, respectively.

The particular case of reciprocal waveguides having identical upper and lower half-spaces must be treated separately since mapping (9) would lead to $R = 0$ and $k_{yu} = \pm k_{yl}$ when $k_u = k_l$. This drawback can be overcome by choosing k_{yu} as the computational variable, which would yield a Riemann surface for the characteristic function comprising two unconnected sheets [13]. This can be understood as an splitting of the characteristic function into the two following functions:

$$\begin{cases} F_{4a}(k_{yu}, \omega) = k_{yu}^2 \det\{\mathbf{L}(k_{yu}, k_{yl}, \omega)\}|_{k_{yl}=-k_{yu}} \\ F_{4b}(k_{yu}, \omega) = k_{yu}^2 \det\{\mathbf{L}(k_{yu}, k_{yl}, \omega)\}|_{k_{yl}=k_{yu}} \end{cases} \quad (17)$$

both of them being analytic in the entire complex k_{yu}-plane. The first one, F_{4a}, accounts for BMs and for improper modes whose corresponding fields grow both upwards in the upper half-space and downwards in the lower half-space. On the other hand, the zeroes of F_{4b} correspond to improper modes whose related fields diverge only in one of the two half-spaces.

Once the fully analytic characteristic functions (4), (6), (16), and (17) have been formulated, the root-searching strategy reported in [27] can be now applied to these functions to compute the propagation constant for the modes of reciprocal waveguides. First, our results will be checked versus some previous results reported in the literature. A first comparison has been carried out with the results presented in [25, Table I] (which, in turn, compares with [14]) for the propagation constant of several leaky modes in a four-layer open isotropic waveguide with different upper and lower half-spaces. An excellent agreement of more than eight identical digits has been always found between our results and those in [25].

Next, a comparison is shown in Fig. 3 for the reciprocal anisotropic dielectric slab surrounded by free space previously studied in [26, Fig. 2]. The slab shows uniaxial anisotropy with permittivity $\varepsilon_{\|}$ along the optical axis and $\varepsilon_{\perp}$ along any direction perpendicular to the optical axis (the orientation of the optical axis is shown in Fig. 3). An excellent agreement has been also found in this case between our numerical results and those reported in [26] for both the proper and improper modes. This figure includes an additional fundamental mode that was not considered in [26].

As a new case study, the proposed method will be now used to compute the complete dispersion relation for the BMs of an anisotropic dielectric layered waveguide with different lower

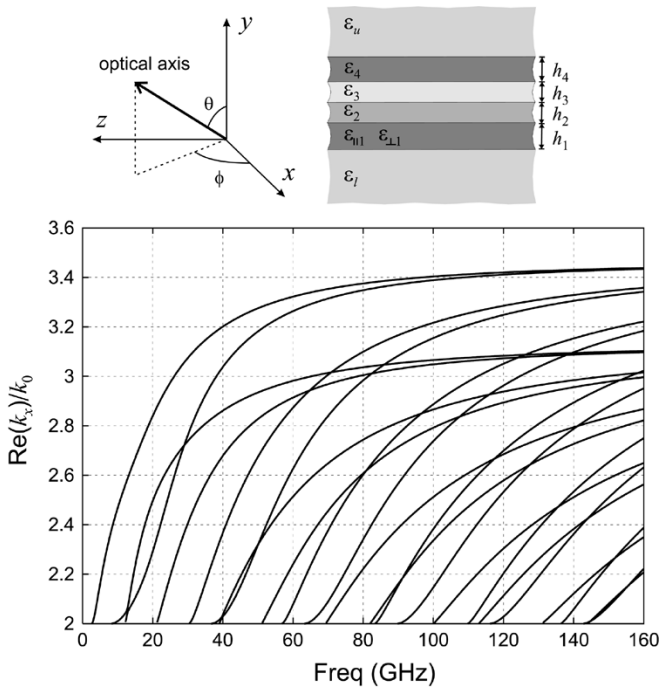

Fig. 4. Normalized propagation constants of the BMs of an open anisotropic reciprocal dielectric waveguide with $h_1 = h_2 = h_3 = h_4 = 2$ mm, $\varepsilon_l = \varepsilon_0, \varepsilon_u = 4\varepsilon_0, \varepsilon_{\parallel 1} = 2.25\varepsilon_0, \varepsilon_{\perp 1} = 4\varepsilon_0, \varepsilon_2 = 9.8\varepsilon_0, \varepsilon_3 = 2.2\varepsilon_0, \varepsilon_4 = 12\varepsilon_0, \theta = \phi = 45°$.

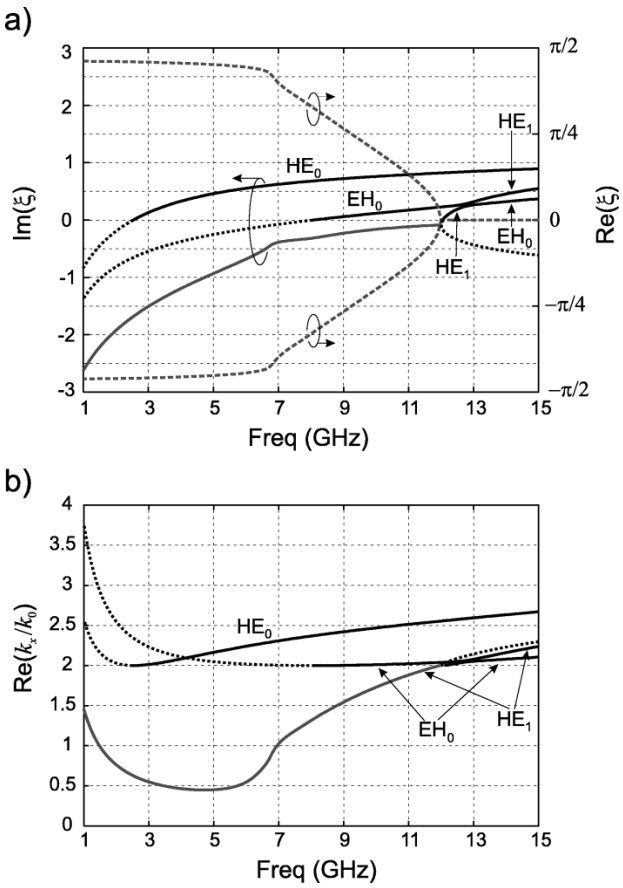

Fig. 5. Frequency evolution of: (a) the imaginary and real parts of ξ and (b) the normalized phase constant of the HE_0, EH_0, and HE_1 modes of the open reciprocal waveguide previously analyzed in Fig. 4. Black solid lines stand for proper mode, black dotted lines for IRM, and grey lines for ICM.

and upper half-spaces. Thus, the layered substrate considered in Fig. 4 has four layers, three of them being isotropic and one presenting uniaxial anisotropy with a tilted optical axis (the orientation of the optical axis has been chosen arbitrarily as $\theta = \phi = 45°$). The data in Fig. 4 have been computed by applying the root-searching algorithm presented in [27] to the analytic characteristic function (16) along the segment of the complex ξ-plane between $\xi = 1.26j$ (which corresponds to $k_x \approx 3.44k_0$) and $\xi = 0$ (i.e., $k_x = 2k_0$). It should be pointed out that all the data corresponding to the 22 modes plotted in Fig. 4 have been obtained automatically without any interaction with the program during execution. Moreover, the algorithm is reliable even in the zones where two or more modes are very close, and no BM is lost in the considered frequency range. In addition, our strategy turns out to be remarkably efficient: the computation of the approximately 9500 values of the propagation constant plotted in Fig. 4 took approximately 11 min on a Pentium IV platform at 2 GHz. An interesting feature of the dispersion curves presented in Fig. 4 is that no BMs are found for frequencies below 2.6 GHz, although the layers of the analyzed structure have permittivities considerably higher than those for the lower and upper half-spaces ($\varepsilon_2 = 9.8\varepsilon_0$ and $\varepsilon_4 = 12\varepsilon_0$ versus $\varepsilon_l = \varepsilon_0$ and $\varepsilon_u = 4\varepsilon_0$).

The above fact can be better appreciated in Fig. 5(a), which shows the evolution as frequency decreases from 15 to 1 GHz of the imaginary and real parts of ξ for the first three BMs and an improper mode of the structure considered in Fig. 4. It can be observed that the second and third modes that are present at 15 GHz (the HE_1 and EH_0 modes, respectively) couple together for a frequency range under 13 GHz. For lower frequencies, the third mode (which is now the HE_1 mode as a consequence of the coupling) keeps on being a proper mode until, at approximately 12.1 GHz, it crosses the real axis of the ξ complex plane to enter the $\Im(k_{yu}) > 0$ zone [see Fig. 2(b)] where it turns into an improper real mode (IRM). This improper mode meets another IRM at 11.9 GHz to give rise to a pair of improper complex modes (ICMs) with the same value of $\Im(\xi)$ and opposite values of $\Re(\xi)$, namely, they are complex conjugate in the k_x plane. As frequency decreases down to 1 GHz, this pair of ICMs stays in the same zone of the ξ complex plane without any further change in the signs of the real and imaginary parts of k_{yu} and k_{yl}. It can also be observed that the EH_0 and HE_0 modes transition into IRMs at 8.1 and 2.6 GHz, respectively. It should be highlighted that the computation of the propagation constant in the neighborhood of a BM-to-IRM modal transition has not raised any troubles because of the appropriate choice of the independent variable. Otherwise, these transitions would have implied the excursion of the modal solution into a different Riemann sheet with the consequent complication in the tracking procedure. This fact is illustrated in Fig. 5(b), which shows the frequency evolution of the normalized phase constants of the modes plotted in Fig. 5(a). This figure shows how the BM's transition into IRMs at $k_x^2 = 4k_0^2$, where they cross the corresponding branch cut in the complex k_x^2-plane to go into the improper sheet. In a similar fashion, it has been the specific root-searching strategy employed here that has allowed for a

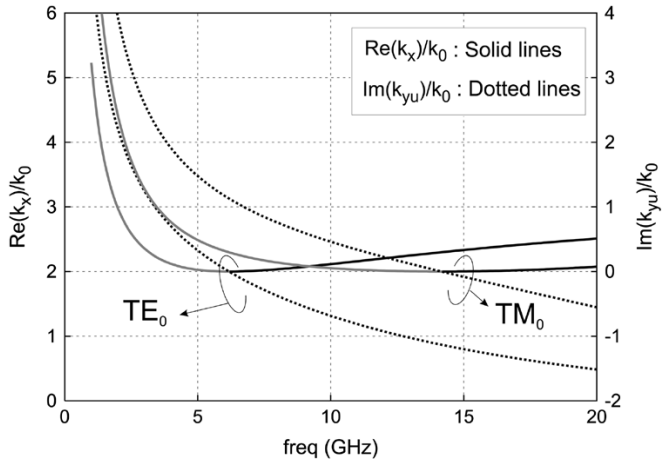

Fig. 6. Normalized propagation constant $\Re(k_x)/k_0$ and imaginary part of the normalized vertical wavenumber of the upper half-space $\Im(k_{yu})/k_0$ of the TE_0 and TM_0 modes of an open isotropic dielectric slab with $h = 2$ mm, $\varepsilon_l = \varepsilon_0, \varepsilon_u = 4\varepsilon_0, \varepsilon_1 = 9.8$. Black solid line denotes the BM and the grey solid line denotes the IRM.

suitable scanning of the regions in which two or more modal solutions have very near locations in the complex plane, e.g., the IRM-to-ICM transitions (splitting points) and the coupling between BMs.

In connection with the previous discussion, it should be highlighted that the lack of BMs at low frequency is not directly related to either the anisotropic nature of the layered substrate or to the specific orientation of the optical axis. Instead, the existence of cutoff frequencies for the first two modes of the structure should be rather related to the presence of different upper and bottom half-spaces, as is well known to happen for the asymmetric slab [39], [40]. In order to clarify this point, the dispersion curves of the TE_0 and TM_0 modes of a single isotropic dielectric slab surrounded by different upper and bottom half-spaces are studied in Fig. 6 (the structure under study is a simplification of the anisotropic layered slab previously considered). This figure shows that both the TE_0 and TM_0 modes are IRMs for low frequencies with cutoff frequencies at approximately 6.20 and 14.2 GHz, respectively. At the cutoff frequencies, it can be observed that the imaginary part of the vertical wavenumber in the upper half-space of the corresponding modes change its sign, thus denoting an improper-to-proper modal transition. A qualitative explanation of the above transition can be given by first considering the slab surrounded by free space (a symmetric slab). In this case, it is well known that the lower the frequency, the larger the evanescent fields of the TE_0 and TM_0 modes spread out in the upper and lower free-space regions. In consequence, their corresponding normalized phase constants approach asymptotically unity for low frequencies ($\Re(k_x)/k_0 \to 1$ as $\omega \to 0$), and these modes do not present cutoff frequencies. If one of the half-spaces is now different from the other (say, e.g., that $\varepsilon_l = \varepsilon_0 < \varepsilon_u$), the field is also expected to spread out in both half-spaces. However, if $k_x^2 \to k_0^2$, the propagation wavenumber will eventually cross the branch point located at $k_x^2 = k_0^2\varepsilon_u/\varepsilon_0$ in its evolution in the complex k_x^2-plane, and, when this crossing takes place, the BM will turn into an IRM. This behavior will always be found for any values of the permittivities of the half-spaces (as long as they are different) and any composition of the layered slab. Thus, and according to the above rationale, it can be concluded that there are not fundamental modes in any kind of layered slab when the upper and lower half-spaces are different.

IV. Nonreciprocal Waveguides

When nonreciprocal materials are involved, the elements of matrix $[\mathbf{A}]$ are not invariant under inversion of the propagation direction and, hence, they are no longer even functions of k_x. For grounded and/or open nonreciprocal waveguides, this fact has important consequences that will be analyzed further here. Nevertheless, the other properties of matrix $[\mathbf{A}]$ mentioned at the beginning of Section III still hold, which causes the characteristic function (4) to be still analytic for shielded and parallel-plate nonreciprocal waveguides. Thus, the root-searching strategy in [27] can also be applied to the characteristic function (4) even if the structure is nonreciprocal (although the independent variable will now be k_x rather than k_x^2). Sections IV-A and B will separately analyze the remaining cases of grounded and open nonreciprocal waveguides.

A. Grounded Nonreciprocal Waveguides

If mapping (5) were now employed, there will be two possible values of $k_x (k_x = \pm\sqrt{k_u^2 - k_{yu}^2})$ for each value of the computational variable k_{yu}. This fact was irrelevant for the case of reciprocal waveguides since the elements of matrices $[\mathbf{A}]$ and $[\mathbf{Z}_u]$ were even functions of k_x. Nevertheless, for nonreciprocal waveguides, this latter parity is lost and, consequently, the ambiguity in the sign of k_x leads to a two-valued characteristic function with a pair of branch points at $k_{yu} = \pm k_u$. Due to the similarity of this situation with that arising for the case of open reciprocal waveguides, the same rationale exposed in Section III-B can be applied here to arrive at the following general mapping:

$$f(\eta) = k_x \pm j k_{yu}. \tag{18}$$

Similar to Section III-B, the above mapping will make the determinant of matrix $\mathbf{L}$ be single-valued and regular provided that $f(\cdot)$ is analytic and that it does not have zeros. In this case, our particular choice will be

$$k_u\, e^{j\eta} = k_x + j k_{yu} \tag{19}$$

which leads to

$$k_x = k_u \cos(\eta) \tag{20}$$

$$k_{yu} = k_u \sin(\eta) \tag{21}$$

$$\eta = -j \ln\left(\frac{k_x + j k_{yu}}{k_u}\right). \tag{22}$$

The following characteristic function is then proposed:

$$F_5(\eta, \omega) = \sin(\eta) \det\{\mathbf{L}(\eta, \omega)\} \tag{23}$$

which present neither poles, nor branch points in the complex η-plane. The reason for choosing this new variable is again that

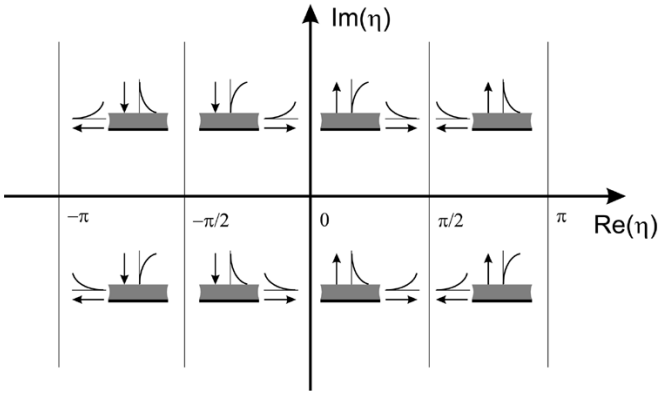

Fig. 7. Schematic representation of the mapping in (19) showing the power flow through the longitudinal and vertical directions (arrows), as well as the exponential behavior of the fields (curves) in each zone of the region of interest of the complex η-plane.

the mapping of the sheets of the original k_x or k_{yu} Riemann surfaces onto the complex η-plane is easy to handle (see Fig. 7). As in Section III-B, the domain of the real part of η is newly restricted to $-\pi < \Re(\eta) \leq \pi$ in order to deal only with the principal value of the complex logarithm. In this case, BMs of lossless waveguides are located on the $[\Re(\eta) = 0, \Im(\eta) < 0]$ segment for forward propagation and on the $[\Re(\eta) = \pi, \Im(\eta) > 0]$ segment for backward propagation (here, forward/backward propagation stands for propagation along the positive/negative x-axis). The effect of losses will be a migration of the forward and backward BMs into the $[-\pi/2 < \Re(\eta) < 0, \Im(\eta) < 0]$ and $[-\pi < \Re(\eta) < -\pi/2, \Im(\eta) > 0]$ zones, respectively.

It is interesting to note that the well-known steepest descent mapping [38], $k_x = k_u \sin(\eta)$, used in [19] and elsewhere, can be viewed as a particular case of the general mapping in (18).

B. Open Nonreciprocal Waveguides

The situation arising for open nonreciprocal waveguides is certainly the most involved. As in the case of open reciprocal waveguides, four-valued characteristic functions in the complex k_x-plane have to be dealt with. Nevertheless, the nonreciprocity of the structure causes that no mapping of the form given in (9) manages to unfold the corresponding Riemann surface. It should be noted that, in the present case, two possible values of k_x will be associated with each value of k_{yu} and k_{yl}, namely, $k_x = \pm\sqrt{k_u^2 - k_{yu}^2} = \pm\sqrt{k_l^2 - k_{yl}^2}$. If the same rationale as in Section III-B was followed, next step would be to study the following linear combination:

$$f(\zeta) = c_1 k_{yu} + c_2 k_{yl} + c_3 k_x \tag{24}$$

in order to infer the conditions under which k_{yu}, k_{yl} and k_x are single-valued functions of ζ. One can proceed by writing both k_{yu} and k_{yl} in terms of k_x and then eliminating the square roots to obtain a fourth-order complex polynomial in k_x. However, it has been found that the coefficients of the second-, third-, and fourth-order terms cannot simultaneously get null and, hence, a mapping as (24) is unable to unfold the Riemann surface.

After studying different possibilities, our best suggestion is to choose mapping (12) to pose the characteristic function as in (16), although F_3 will now be a two-valued function

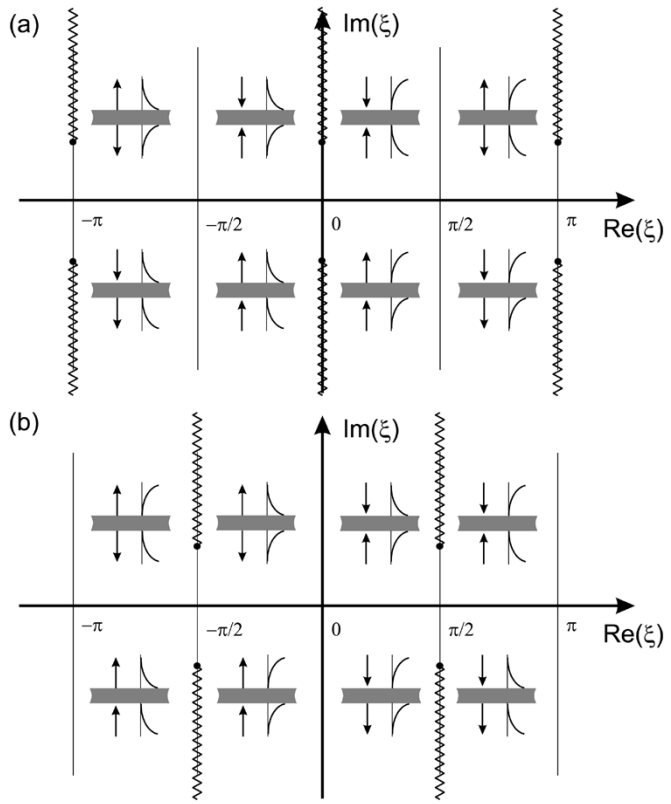

Fig. 8. Schematic representation of the region of interest in the complex ξ-plane for open nonreciprocal waveguides when: (a) $k_l > k_u$ and (b) $k_u > k_l$. The branch points correspond to $k_x = 0$ and the branch cuts are defined as $\Re(k_x) = 0$.

without poles. The corresponding complex ξ-plane will then be a two-sheeted Riemann surface with branch points at $\xi = \arcsin(\pm j k_u/R)$ or, equivalently, $\xi = \arccos(\pm k_l/R)$, corresponding to $k_x = 0$. Taking the branch cuts lying along the $\Re(k_x) = 0$ loci, the upper sheet will define forward propagation $(\Re(k_x) > 0)$, whereas the lower sheet will correspond to backward propagation $(\Re(k_x) < 0)$. The resulting two-sheeted Riemann surface is depicted in Fig. 8.

Note that either η in (18) or a linear combination of k_x and k_{yl} could also have been chosen as the computational variable. Nevertheless, these latter choices would have led to inconvenient Riemann surfaces with branch points at $k_{yl} = 0$ and $k_{yu} = 0$, respectively. These two points are of great interest when performing a root searching since some modal propagation constants are expected to appear in their neighborhood. For example, the transitions from IRMs to BMs in lossless waveguides take place at $k_{yl} = 0$ for $k_l > k_u$ and at $k_{yu} = 0$ for $k_u > k_l$ (in other words, these are precisely the cutoff points). Another disadvantage of the above variables would have been the rather probable situation of a mode crossing a branch cut and entering the other sheet of the Riemann surface during its possible evolution. This fact would have considerably complicated the tracking of the modal solutions, e.g., in a frequency sweep. On the contrary, the proposed mapping (12) makes the neighborhood of the corresponding branch points be regions of scarce physical interest (no modes are generally expected in the vicinity of $k_x = 0$), which will greatly help to simplify the root-searching procedure. In addition, the choice of the branch

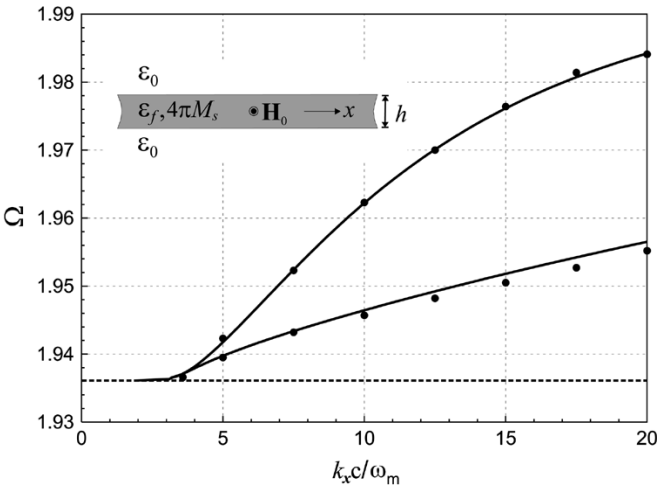

Fig. 9. Dispersion curve $\Omega(k_x)$ of the surface-wave mode in [8, Fig. 1] ($\Omega = \omega/\omega_m, \omega_m = 4\pi\gamma M_s$). The slab ferrite is characterized by $\varepsilon_f = 15.4\varepsilon_0, 4\pi M_s = 1760$ G, $\mathbf{H}_0 = 2640\hat{\mathbf{z}}$(Oe), and a height of $h = 0.15c/\omega_m$. Solid lines: our results. Points: data in [8].

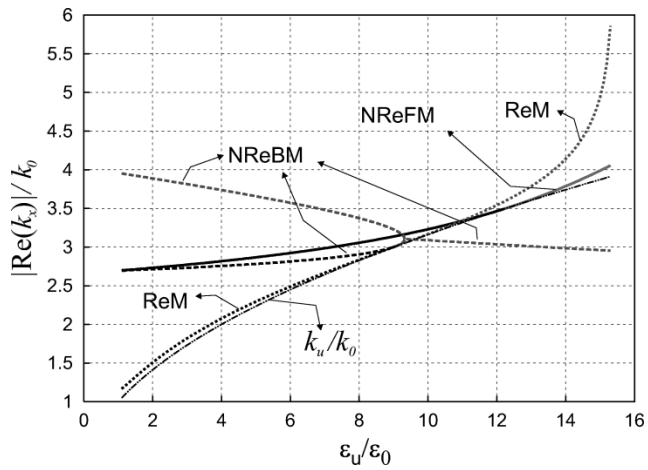

Fig. 10. Behavior of the magnitude of the normalized propagation constant for the forward and backward first modes of an open ferrite slab as the relative permittivity of the upper half-space ($\varepsilon_u/\varepsilon_0$) is varied. Structural parameters: $\varepsilon_l = \varepsilon_0, \varepsilon_r = 15.4, 4\pi M_s = 1760$ G, $\mathbf{H}_0 = 2640\,\hat{\mathbf{z}}$ (Oe), $h = 1.45$ mm, and $\mathrm{Freq} = 20$ GHz. Black color stands for proper modes and grey color for improper ones. $(\cdots)$: Reciprocal mode (ReM), $(- - - - -)$: Nonreciprocal backward Mode (NReBM), (————): Nonreciprocal forward mode (NReFM).

cuts along $\Re(k_x) = 0$ will also prevent the appearance of special difficulties when tracking a modal solution. Certainly, the modes are not expected to change their forward/backward nature in their possible evolution and, therefore, the roots of the characteristic function are not expected to cross the branch cuts. Thus, by choosing ξ as the computational variable, one only needs to select forward/backward propagation and the application of the root-searching procedure described in [27] to the characteristic function $F_3(\xi)$ will be rather effective and reliable in spite of the presence of the branch points.

It should be mentioned that, in those cases where nonreciprocity is induced by an external biasing field, the searching for forward- and backward-propagating modes can be circumscribed to just one of the sheets of the Riemann surface. If this sheet is chosen as the forward-propagation one, the backward-propagating modes can be readily computed by simply reversing the biasing field. Due to this fact, and taking into account that the presence of the branch points/cuts will only exceptionally pose any problem to the tracking process, it has been possible to find a quite similar procedure to deal with open layered waveguides involving magnetized ferrites as that for open dielectric waveguides.

Previous to using the current approach to study some novel structures, a comparison of our results with those reported in [8] for the surface-wave dispersion curves of a ferrite slab surrounded by free space is first presented in Fig. 9. This figure shows a good agreement between the two sets of data (relative differences smaller than 0.1%), which confirms the suitability of the current method to study open nonreciprocal structures.

Our approach is now applied to study some details of the modal evolution in the same ferrite slab previously analyzed in Fig. 9, although now with an upper dielectric half-space of permittivity ε_u. Thus, Fig. 10 shows the behavior of the normalized phase constants of both the forward and backward first modes as the relative permittivity of the upper half-space $(\varepsilon_u/\varepsilon_0)$ varies from unity up to the value corresponding to the ferrite slab. The propagation constants of the backward modes are computed in the forward-propagation sheet of the Riemann surface by simply changing the sign of the x and z components of the biasing field (namely, using $\phi+\pi$ instead of ϕ for the biasing magnetic field). For the case of the symmetric slab $(\varepsilon_u = \varepsilon_0)$, two pairs of forward/backward proper modes are found. The pair of modes with the smaller propagation constant is, in fact, a reciprocal mode (ReM) (dotted line), and then it shows the same magnitude of the propagation constant for both the forward and backward modes. As ε_u increases, the propagation constant of this mode touches the curve of $k_u/k_0 (k_u = \omega\sqrt{\varepsilon_u\mu_0})$ at $\varepsilon_u/\varepsilon_0 \approx 9.2$ (in the complex k_x-plane, the k_x solution touches the branch point associated with the upper half-space), where this proper mode turns into an IRM. (The proper/improper nature of the modes is marked by black/grey color of the corresponding curve.) At low values of $\varepsilon_u/\varepsilon_0$, there also appears another pair of nonreciprocal modes, which increases its nonreciprocity for larger values of ε_u. The curve corresponding to the nonreciprocal forward mode (NReFM) (solid line) touches the k_u/k_0 curve at $\varepsilon_u/\varepsilon_0 \approx 12.2$ to transition, at this point, into an IRM. As for the nonreciprocal backward mode (NReBM) (dashed line), its dispersion curve touches the k_u/k_0 curve at $\varepsilon_u/\varepsilon_0 \approx 9.31$ where the mode transitions into an IRM to further meet another IRM at $\varepsilon_u/\varepsilon_0 \approx 9.06$ to give rise to a complex leaky mode.

Next, Fig. 11 shows another study example that analyzes the evolution in the complex ξ-plane of a proper mode of an open ferrite slab for frequencies ranging from 1 to 50 GHz. In this case, the external magnetizing field does not coincide with any of the Cartesian axes of the structures. This situation is well known to complicate the posing of a closed-form characteristic equation; in fact, this equation is usually found numerically after the transverse matrix method is employed (see, e.g., [19]). The root searching has been carried out in the $\Re(k_x) > 0$ sheet and, hence, the modes plotted in Fig. 11 propagate forward along the x-direction. As frequency decreases from 50 GHz, it can be observed that the proper mode crosses the real axis at 32.7 GHz and enters the $\Im(k_{yl}) < 0$ zone to become an improper mode. As

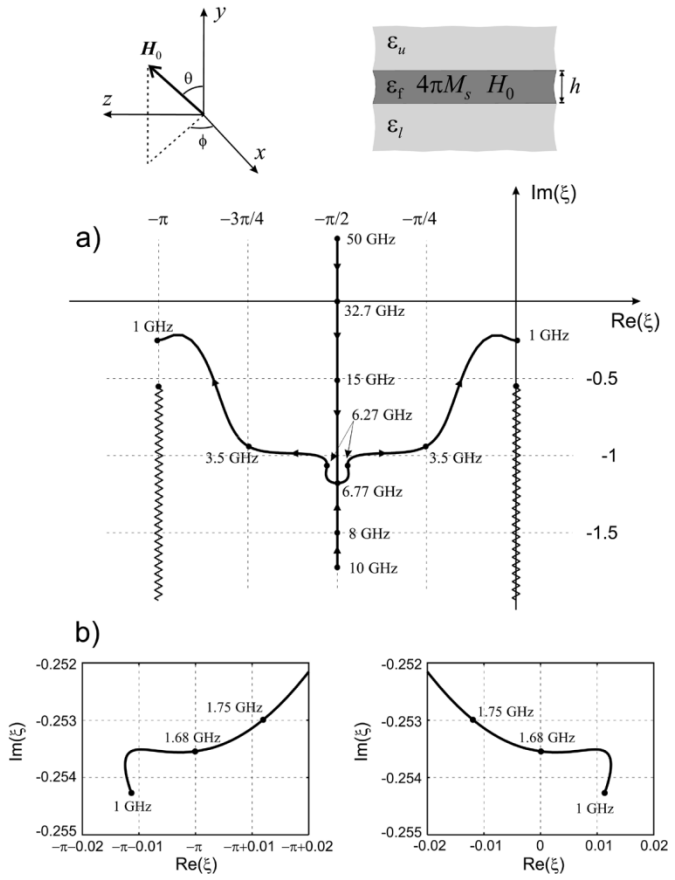

Fig. 11. (a) Evolution in the complex ξ-plane of two modal solutions of the depicted open nonreciprocal waveguide. (b) Closer view of the evolution of the two plotted modes near 1 GHz. The parameters of the structure are $\varepsilon_l = 4\varepsilon_0, \varepsilon_u = \varepsilon_0, h = 0.635$ mm, $\varepsilon_f = 15\varepsilon_0$, $4\pi M_s = 800$ G, $H_0 = 500$ Oe, $\phi = 90°$, and $\theta = 45°$. The branch cuts are also shown and the arrows point in the direction of decreasing frequencies.

long as this mode has $\Re(\xi) = -\pi/2$, it is an IRM. Another IRM has been plotted for frequencies below 10 GHz. Both IRMs meet together at 6.77 GHz, giving rise to a pair of complex modes: the mode having $\Re(\xi) < \pi/2$ is a downward-leaky mode (i.e., a mode that leaks into the lower half-space), while the other one is its corresponding complex conjugate in the k_x-plane. For lower frequencies, this pair of k_x-complex-conjugate modes further evolve in the complex ξ-plane until, at approximately 1.68 GHz, they cross the $\Re(\xi) = -\pi$ line and the imaginary axis, respectively [see the closer view in Fig. 11(b)]. At this frequency, the right-most mode transitions into a upward-leaky mode, whereas the former downward-leaky mode now becomes the k_x-complex-conjugate of the new upward-leaky mode. It should be highlighted that the choice of a suitable independent variable together with a proper definition of the branch cuts has greatly simplified the computation of the modal solutions in the near vicinity of the latter modal transitions (the modal solutions have not crossed any branch cut in their evolution in the complex ξ-plane). Concerning the splitting point (IRM-to-ICM transition), the specific root-searching strategy has again allowed for a straightforward tracking of both modal solutions as they get closer to each other.

Finally, Fig. 12 shows the normalized phase constant of the forward modes in Fig. 11 in the vicinity of the splitting point

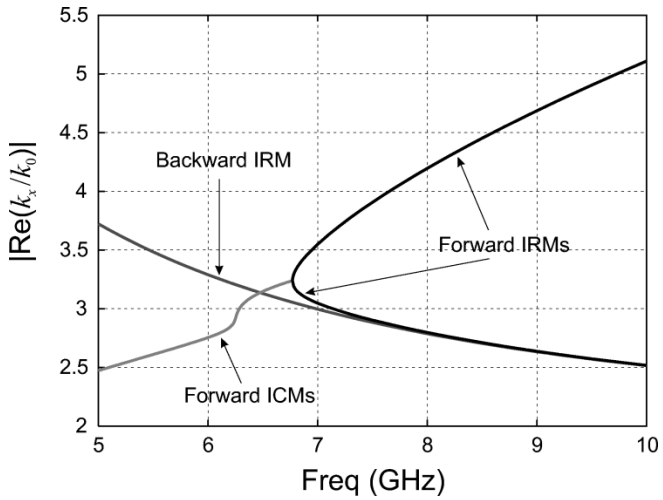

Fig. 12. Detail of the splitting point of Fig. 11 also showing a backward IRM.

appearing at 6.77 GHz. In addition, the magnitude of the normalized phase constant of a backward IRM is also shown (its phase constant is negative). It can be observed how both the forward and backward modes are almost indistinguishable (i.e., the effect of the nonreciprocity is almost negligible) for frequencies beyond 8 GHz. However, for lower frequencies, their behaviors are clearly different. Specifically, the forward mode transition into an ICM, whereas the backward mode does not go through any splitting point and, hence, does not suffer any transition in this frequency range.

V. Conclusion

This paper has addressed the general problem of posing the transcendental equations of planar layered waveguides in its most convenient form. Since the root-searching methods work more efficiently when dealing with analytic functions, a general theoretical discussion on the most suitable mapping (if any) for each type of waveguides: shielded, parallel-plate, grounded, and open reciprocal/nonreciprocal waveguides (including the case of different upper and lower half-spaces) has been presented. For shielded and parallel-plate waveguides, the characteristic function formulated here is directly analytic when the wavenumber along the propagation direction is used as the independent variable. If the structure under study is a grounded reciprocal/nonreciprocal waveguide or an open reciprocal waveguide, an appropriate mapping that unfolds the longitudinal-wavenumber Riemann surface is proposed, and a corresponding analytic characteristic function is formulated in each case. For the case of open nonreciprocal waveguides, no mapping has been found to unfold the Riemann surface. Nevertheless, an effective approach has been proposed to deal with these structures. In particular, the case of open layered waveguides containing magnetized ferrites has been set up in a similar fashion as the case of dielectric waveguides. Thus, the modal solutions will not cross any branch cut in their evolution with respect to some parameter of the structure and, hence, their tracking is rather straightforward even if they transition into different nature modal solutions. The combination of the proposed formulation of the characteristic equation with a convenient integral-na-

ture root-searching method makes possible the systematic analysis of a given region of the complex plane. This allows for an automatic searching for the roots within the region, even when modal couplings and splitting points appear. Some numerical results have been presented for reciprocal and nonreciprocal open waveguides to show the good performance of the proposed formulation.

REFERENCES

[1] R. Seckelmann, "Propagation of TE modes on dielectric loaded waveguides," *IEEE Trans. Microw. Theory Tech.*, vol. MTT-14, no. 11, pp. 518–527, Nov. 1966.

[2] F. E. Gardiol, "Higher-order modes in dielectrically loaded rectangular waveguides," *IEEE Trans. Microw. Theory Tech.*, vol. MTT-16, no. 11, pp. 919–924, Nov. 1968.

[3] T. J. Gerson and J. S. Nadan, "Surface electromagnetic modes of a ferrite slab," *IEEE Trans. Microw. Theory Tech.*, vol. MTT-22, no. 8, pp. 757–763, Aug. 1974.

[4] Y. Suematsu and K. Furuya, "Quasiguided modes and related radiation losses in optical dielectric waveguides with external higher index surroundings," *IEEE Trans. Microw. Theory Tech.*, vol. MTT-23, no. 1, pp. 170–175, Jan. 1975.

[5] M. S. Sodha and N. C. Srivastava, *Microwave Propagation in Ferrimagnetics*. New York: Plenum, 1981.

[6] S. Talisa, "Application of Davidenko's method to the solution of dispersion relations in lossy waveguide systems," *IEEE Trans. Microw. Theory Tech.*, vol. MTT-33, no. 10, pp. 967–971, Oct. 1985.

[7] M. A. Morgan, D. L. Fisher, and E. A. Milne, "Electromagnetic scattering by stratified inhomogeneous anisotropic media," *IEEE Trans. Antennas Propag.*, vol. AP-35, no. 2, pp. 191–197, Feb. 1987.

[8] R. Ruppin, "Electromagnetic modes of a ferrite slab," *J. Appl. Phys.*, vol. 62, pp. 11–15, Jul. 1987.

[9] W. C. Chew, *Waves and Fields in Inhomogeneous Media*, 2nd ed. Piscataway, NJ: IEEE Press, 1995.

[10] M. A. Marin, S. Barkeshli, and P. H. Pathak, "On the location of proper and improper surface wave poles for the grounded dielectric slab," *IEEE Trans. Antennas Propag.*, vol. 38, no. 4, pp. 570–573, Apr. 1990.

[11] C.-I. G. Hsu, R. F. Harrington, J. R. Mautz, and T. P. Sarkar, "On the location of leaky waves poles for a grounded dielectric slab," *IEEE Trans. Microw. Theory Tech.*, vol. 39, no. 2, pp. 346–349, Feb. 1991.

[12] V. A. Labay and J. Bornemann, "Matrix singular-value decomposition for pole-free solutions of homogeneous matrix equations as applied to numerical modeling methods," *IEEE Microw. Guided Wave Lett.*, vol. 2, no. 2, pp. 49–51, Feb. 1992.

[13] R. E. Smith, N. S. Houde-Walter, and G. W. Forbes, "Mode determination of planar waveguides using the four-sheeted dispersion relation," *IEEE J. Quantum Electron.*, vol. 28, no. 6, pp. 1520–1526, Jun. 1992.

[14] E. Anemogiannis and E. N. Glytsis, "Multilayer waveguides: Efficient numerical analysis of general structures," *J. Lightwave Technol.*, vol. 10, no. 10, pp. 1344–1351, Oct. 1992.

[15] H. A. N. Hejase, "On the use of Davidenko's method in complex root search," *IEEE Trans. Microw. Theory Tech.*, vol. 41, no. 1, pp. 141–143, Jan. 1993.

[16] R. Marqués, F. Mesa, and M. Horno, "Nonreciprocal and reciprocal complex and backward waves in parallel plate waveguides loaded with a ferrite slab arbitrarily magnetized," *IEEE Trans. Microw. Theory Tech.*, vol. 41, no. 8, pp. 1409–1418, Aug. 1993.

[17] R. E. Smith, G. W. Forbes, and N. S. Houde-Walter, "Unfolding the multivalued planar waveguide dispersion relation," *IEEE J. Quantum Electron.*, vol. 29, no. 4, pp. 1031–1034, Apr. 1993.

[18] R. E. Smith and N. S. Houde-Walter, "The migration of bound and leaky solutions to the waveguide dispersion relation," *J. Lightwave Technol.*, vol. 11, no. 11, pp. 1760–1768, Nov. 1993.

[19] F. Mesa and M. Horno, "Computation of proper and improper modes in multilayered bianisotropic waveguides," *IEEE Trans. Microw. Theory Tech.*, vol. 43, no. 1, pp. 233–235, Jan. 1995.

[20] A. Bakhtazad, H. Abiri, and R. Ghayour, "A general transform for regularizing planar open waveguide dispersion relation," *J. Lightwave Technology*, vol. 15, no. 2, pp. 383–390, Feb. 1997.

[21] S. Amari and J. Bornemann, "A pole-free modal field-matching technique for eigenvalue problems in electromagnetics," *IEEE Trans. Microw. Theory Tech.*, vol. 45, no. 9, pp. 1649–1653, Sep. 1997.

[22] Y. Long and H. Jiang, "Numerical analysis of surface wave on microstrip antenna with lossy substrate," *Electron. Lett.*, vol. 33, pp. 1016–1021, Sep. 1997.

[23] E. Anemogiannis, E. N. Glytis, and T. K. Gaylord, "Determination of guided and leaky modes in lossless and lossy planar multilayer optical waveguides: Reflection pole method and wavevector density method," *J. Lightwave Technol.*, vol. 17, no. 5, pp. 929–941, May 1999.

[24] S.-A. Teo, M.-S. Leong, S.-T. Chew, and B.-L. Ooi, "Complete location of poles for thick lossy grounded dielectric slab," *IEEE Trans. Microw. Theory Tech.*, vol. 50, no. 2, pp. 440–445, Feb. 2002.

[25] J. Petrácek and K. Singh, "Determination of leaky modes in planar multilayer waveguides," *IEEE Photon. Technol. Lett.*, vol. 14, no. 6, pp. 810–812, Jun. 2002.

[26] A. B. Yakovlev and G. W. Hanson, "Fundamental modal phenomena on isotropic and anisotropic planar slab dielectric waveguides," *IEEE Trans. Antennas Propag.*, vol. 51, no. 4, pp. 888–897, Apr. 2003.

[27] R. Rodríguez-Berral, F. Mesa, and F. Medina, "Systematic and efficient root finder for computing the modal spectrum of planar layered waveguides," *Int. J. RF Microwave Computer-Aided Eng.*, vol. 14, pp. 73–83, Jan. 2004.

[28] Y. L. Chow, J. J. Yang, D. G. Fang, and G. E. Howard, "A closed-form spatial Green's function for the thick microstrip substrate," *IEEE Trans. Microw. Theory Tech.*, vol. 39, no. 3, pp. 588–592, Mar. 1991.

[29] J. Bernal, F. Mesa, and F. Medina, "2-D analysis of leakage in printed-circuit lines using discrete complex-images technique," *IEEE Trans. Microw. Theory Tech.*, vol. 50, no. 8, pp. 1895–1900, Aug. 2002.

[30] I. Y. Hsia and N. G. Alexopoulos, "Radiation characteristics of Hertzian dipole antennas in a nonreciprocal superstrate–substrate structure," *IEEE Trans. Antennas Propag.*, vol. 40, no. 7, pp. 782–790, Jul. 1992.

[31] P. Baccarelli, A. Galli, C. Di Nallo, F. Frezza, and P. Lampariello, "Attractive features of leaky-wave antennas based on ferrite-loaded open waveguides," in *IEEE MTT-S Int. Microwave Symp. Dig.*, 1997, pp. 1442–1445.

[32] P. Baccarelli, C. Di Nallo, F. Frezza, A. Galli, and P. Lampariello, "Propagation and radiation characteristics of gyrotropic open structures in the presence of sources," in *IEEE MTT-S Int. Microwave Symp. Dig.*, 1998, pp. 655–658.

[33] L. M. Delves and J. L. Lyness, "A numerical method for locating the zeros of an analytic function," *Math. Comput.*, vol. 21, pp. 543–560, Oct. 1967.

[34] P. Lampariello and R. Sorrentino, "The ZEPLS program for solving characteristic equations of electromagnetic structures," *IEEE Trans. Microw. Theory Tech.*, vol. MTT-23, no. 5, pp. 457–458, May 1975.

[35] C. M. Krowne, "Fourier transformed matrix method of finding propagation characteristics of complex anisotropic layered media," *IEEE Trans. Microw. Theory Tech.*, vol. MTT-32, no. 12, pp. 1617–1625, Dec. 1984.

[36] S. C. Tsalamengas and N. K. Uzunoglu, "Radiation from a dipole in the proximity of a general anisotropic grounded layer," *IEEE Trans. Antennas Propag.*, vol. AP-33, no. 2, pp. 165–172, Feb. 1985.

[37] F. Mesa, R. Marqués, and M. Horno, "A general algorithm for computing the bidimensional spectral Green's dyad in multilayered complex bianisotropic media: The equivalent boundary method," *IEEE Trans. Microw. Theory Tech.*, vol. 39, no. 9, pp. 1640–1649, Sep. 1991.

[38] L. B. Felsen and N. Marcuvitz, *Radiation and Scattering of Waves*, 2nd ed. New York: IEEE Press, 1995.

[39] H.-G. Unger, *Planar Optical Waveguides and Fibers*. Oxford, U.K.: Clarendon Press, 1977.

[40] A. W. Snyder and J. D. Love, *Optical Waveguide Theory*. London, U.K.: Chapman & Hall, 1996.

Raúl Rodríguez-Berral was born in Casariche, Seville, Spain, on August 1978. He received the Licenciado degree in physics from the Universidad de Sevilla, Seville, Spain, in 2001, and is currently working toward the Ph.D. degree at the Universidad de Sevilla.

In January 2002, he joined the Departamento de Física Aplicada 1, Universidad de Sevilla.

Mr. Rodríguez-Berral was the recipient of a Spanish Ministry of Science and Technology Scholarship.

Francisco Mesa (M'94) was born in Cádiz, Spain, in April 1965. He received the Licenciado and Doctor degrees from the Universidad de Sevilla, Seville, Spain, in 1989 and 1991, respectively, both in physics.

He is currently an Associate Professor with the Departamento de Física Aplicada 1, Universidad de Sevilla. His research interest focuses on electromagnetic propagation/radiation in planar lines with general anisotropic materials.

Francisco Medina (M'90–SM'01) was born in Puerto Real, Cádiz, Spain, in November 1960. He received the Licenciado and Doctor degrees from the Universidad de Sevilla, Seville, Spain, in 1983 and 1987, respectively, both in physics.

From 1986 to 1987, he spent the academic year with the Laboratoire de Microondes de l'ENSEEIHT, Toulouse, France. From 1985 to 1989, he was a Profesor Ayudante (Assistant Professor) with the Departamento de Electrónica y Electromagnetismo, Universidad de Sevilla, and since 1990, he has been a Profesor Titular (Associate Professor) of electromagnetism. He is also currently Head of the Grupo de Microondas, Universidad de Sevilla. His research interests include analytical and numerical methods for planar structures (transmission lines, circuits and antennas) and the study of the electromagnetism of (bi)anisotropic media and metamaterials. He is reviewer of a number of international scientific and technical journals and local conferences.

Dr. Medina was a member of the Technical Program Committee (TPC) of the 23rd European Microwave Conference, Madrid, Spain, 1993, the TPC of ISRAMT, Malaga, Spain, 1999, and the TPC of the Microwaves Symposiun, Tetouan, Morocco, 2000.